JBIC Journal of Biological Inorganic Chemistry (2020) 25:441–449
https://doi.org/10.1007/s00775-020-01774-3

ORIGINAL PAPER

Targeted cancer cell delivery of arsenate as a reductively activated prodrug

Daniela Cioloboc[1] · **Donald M. Kurtz Jr.**[1]

Received: 9 January 2020 / Accepted: 4 March 2020 / Published online: 18 March 2020

Abstract

Nanoformulations, prodrugs, and targeted therapies are among the most intensively investigated approaches to new cancer therapeutics. Human ferritin has been used extensively as a nanocarrier for the delivery of drugs and imaging agents to cancerous tumor cells both in vitro and in vivo. We report exploitation of the native properties of ferritin, which can be co-loaded with simple forms of iron (FeOOH) and arsenic (arsenate) in place of the native phosphate. The As(III) form arsenic trioxide has been successfully used to treat one blood cancer, but has so far proven too systemically toxic for use on solid tumors in the clinic. The As(V) form, arsenate, on the other hand, while much less systemically toxic upon bolus injection has also proven ineffective for cancer therapy. We extended the C-terminal ends of the human ferritin subunits with a tumor cell receptor targeting peptide and loaded this modified ferritin with ~ 800 arsenates and ~ 1100 irons. Our results demonstrate targeting and uptake of the iron, arsenate-loaded modified human ferritin by breast cancer cells. At the same arsenic levels, the cytotoxicity of the iron, arsenate-loaded human ferritin was equivalent to that of free arsenic trioxide and much greater than that of free arsenate. The iron-only loaded human ferritin was not cytotoxic at the highest achievable doses. The results are consistent with the receptor-targeted human ferritin delivering arsenate as a reductively activated 'prodrug'. This targeted delivery could be readily adapted to treat other types of solid tumor cancers.

Graphic abstract

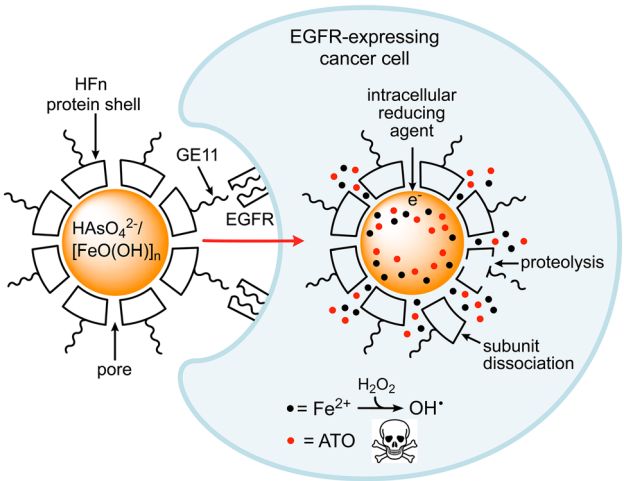

Keywords Arsenic trioxide · Cancer therapy · Ferritin · Nanotechnology

Electronic supplementary material The online version of this article (https://doi.org/10.1007/s00775-020-01774-3) contains supplementary material, which is available to authorized users.

Extended author information available on the last page of the article

Introduction

Arsenic (As) has a long history as both drug and poison [1–3]. The most common therapeutic form of arsenic, arsenic trioxide, As_2O_3 (ATO), can enter cells via passive transport as $As(OH)_3$ [2, 4]. Among other diseases, cancer has been a target of arsenic drugs. One blood cancer has been successfully treated with ATO, but neither ATO nor other arsenic drugs have been clinically successful in treating solid cancer tumors. A stumbling block has been that, to penetrate solid tumors, higher, systemically toxic dosages of ATO are required. These higher ATO concentrations are also difficult to maintain due to rapid renal clearance. Synthetic nanoparticles containing various formulations of ATO were found to enter cells via endocytosis and to improve antitumor efficacy while attenuating systemic toxicity in murine xenograft models [5–9].

ATO and all other current arsenic drugs contain reduced forms of arsenic, typically As(III). Another common form of inorganic arsenic, arsenate ($H_2AsO_4^-$/$HAsO_4^{2-}$ at neutral pH), contains As(V), and arsenate is much less systemically toxic than ATO [2]. Arsenate could conceivably be used as a reducible "prodrug", but we have found no reports of the therapeutic use of arsenate (or any other As(V) compound).

We constructed a platform for cancer cell-targeted arsenate delivery based on the 24-subunit iron storage protein, human H-ferritin (HFn) (Fig. 1a) [10]. The ~ 8-nm hollow cavity of HFn (Fig. 1b) can be artificially loaded with up to ~ 3000 irons as an amorphous ferric oxyhydroxide polymer ($[FeO(OH)]_n$). Our strategy, diagrammed in Fig. 2, is based on the observation that ferritin can be artificially co-loaded with ~ 1700 irons as $[FeO(OH)]_n$ and ~ 800 arsenates per 24-mer [11]. (The arsenate loading does not occur without iron.) In iron-only loaded ferritins the $[FeO(OH)]_n$ can be mobilized by reduction to Fe^{2+} [10], and, based on redox potentials, arsenate is easier to reduce than $[FeO(OH)]_n$ [12, 13]. The hypoxic environment of many tumors could, therefore, promote reduction of arsenate to the more toxic ATO. Another potential arsenic release mechanism stems from the observation that intravenously injected human heavy chain ferritin (HFn) is taken up by lysosomes [14], within which the acidic pH and proteolytic activity are known to promote HFn degradation and to facilitate iron release [15].

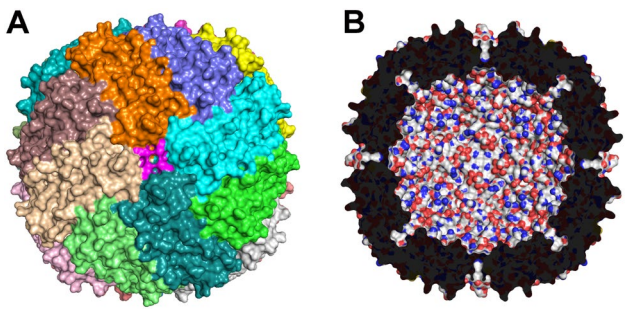

Fig. 1 Structural features of Hfn. **a** Outer surface with the 24 identical subunits distinguished by color and magenta color highlighting one of six sets of four C-termini surrounding a fourfold rotation axis. **b** Cross section of the 24-mer showing the ~ 8-nm internal cavity. Drawings used coordinates from Protein Data Bank entry 3ajo [16]

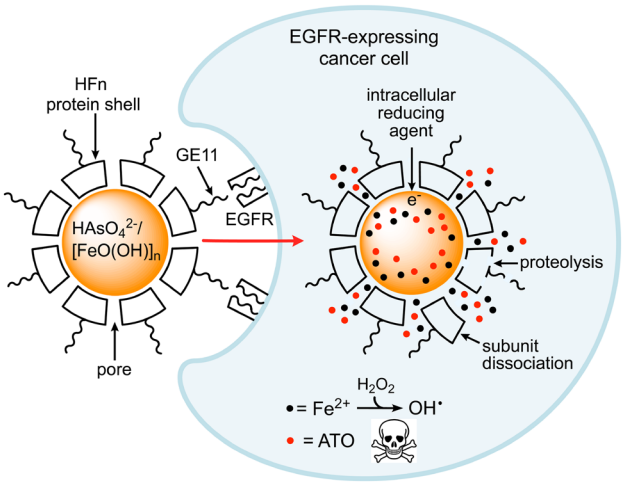

Fig. 2 Arsenic and iron prodrug delivery strategy

HFn has been used for delivery of drugs and imaging agents to tumors [17]. When injected intravenously, HFn was shown to localize to mouse tumor xenografts from commercial cancer cell lines [14]. This localization was attributed to the enhanced permeability and retention effect and to HFn's affinity for transferrin receptor 1, Trf1 [14, 18]. Targeting of HFn to other receptors that are specifically overexpressed in particular types of cancers could conceivably increase the chances of achieving clinically effective therapies. For HFn, a simple targeting strategy has been to extend the protruding N- or C-terminal ends of the 24 identical subunits with known tumor targeting peptides [17, 19–23]. The epidermal growth factor receptor (EGFR) is known to be hyperexpressed in many cancers [24], including a significant percentage of triple-negative breast cancers, which are particularly aggressive [25–27]. GE11 designates a 12-residue peptide, which, when attached to synthetic nanoparticles, was shown to target but not activate EGFR and to induce uptake of the nanoparticles by endocytosis [28–30]. For binding to EGFR, the GE11 peptide has typically been attached to the nanoparticle via its N-terminal end. As diagrammed in Fig. 2, we, therefore, extended the GE11 peptide from the protruding C-terminal ends of the Hfn subunits (Fig. 1a) and tested the Hfn-GE11's ability to deliver arsenic and iron to two breast cancer cell lines.

Materials and methods

Reagents and general procedures

Reagents and buffers were of the highest grade commercially available. All reagents, protein, and media solutions were prepared using water purified with a Millipore ultrapurification system to a resistivity of 18 MΩ to minimize trace metal ion contamination. Unless otherwise stated, all chemicals were purchased from Sigma-Aldrich, LLC, Saint Louis, MO, USA.

HFn expression plasmids

Expression plasmids containing genes encoding either HFn or HFn-GE11 were synthesized by GenScript, Inc. (Piscataway, NJ, USA). The encoding nucleotide sequences were inserted into the 5′NdeI and 3′BamHI restriction sites of the *E. coli* expression plasmid, pT7-7 [31]. The HFn-GE11 plasmid encoded the amino acid sequence: MTTASTSQVRQNYHQDSEAAINRQINLELYASYVYLSMSYYFDRDDVALKNFAKYFLHQSHEEREHAEKLMKLQNQRGGIFLQDIKKPDCDDWESGLNAMECALHLEKNVNQSLLELHKLATDKNDPHLCDFIETHYLNEQVKAIKELGDHVTNLRKMGAPESGLAEYLFDKHTLGDSDNES*GGGSGGGTGGGSGGGYHWYGYTPQNVI*, listed as the N- to C-terminal HFn sequence followed by a 15-residue glycine-rich spacer [19] (italicized) connected to the GE11 sequence (bolded).

Protein overexpression, purification, and characterization

Escherichia coli BL21(DE3) competent cells (Invitrogen) were transformed with either the HFn- or HFn-GE11-encoding plasmids. The proteins were expressed from 1 L cultures of these transformed strains in Luria–Bertani broth containing 100 mg/L ampicillin (LB/amp) at 37 °C. When the OD_{600} of the 1 L cultures reached 0.6–0.8, 1 mL of 100 mg/mL of isopropyl-beta-D-thiogalactoside was added to induce protein expression. These 1 L cultures were incubated for an additional 4 h with shaking at 37 °C. Cells were then harvested by centrifugation at 4 °C and frozen at − 80 °C.

For isolation of HFn, the thawed cell pellet was resuspended in 25 mL of 50 mM 3-(*N*-morpholino)propanesulfonic acid (MOPS), pH 7.3, containing 250 mM NaCl, and 2 mM β-mercaptoethanol, pH 7.3. The resuspended cells were lysed on ice by sonication and cellular debris was removed by centrifugation. The supernatant was heated at 60 °C for 15 min, followed by 30 min centrifugation at 20,000*g* to remove precipitate. The supernatant was loaded on S200 Sephacryl® gel filtration XK16/100 column (GE HealthCare Life Sciences) that had been pre-equilibrated with 50 mM MOPS, pH 7.3, 250 mM NaCl, 2 mM β-mercaptoethanol. Protein content of eluted fractions was assessed by glycine sodium dodecyl sulfate-polyacrylamide gel electrophoresis (SDS-PAGE). The HFn-containing fractions were pooled and concentrated by buffer exchange into 50 mM MOPS, pH 7, and stored at − 80 °C.

For isolation of HFn-GE11 after cell lysis and centrifugation, the supernatant was treated with 50 µg/mL of DNAse and RNAse and 5 mM $MgSO_4$ at room temperature for 30 min, filtered through a 0.22-µm pore membrane, then loaded into a 5-mL HiTrap Q anion-exchange column (GE Healthcare Life Sciences) equilibrated with 50 mM MOPS, pH 7.3. The column was washed with 50 mL of 50 mM MOPS, pH 7.3, and the protein was eluted with 200 mL of a two-step linear gradient of 0–0.2 M NaCl and 0.2–1 M NaCl in the same buffer. Protein content of eluted fractions was assessed by SDS-PAGE, and fractions containing HFn-GE11 were pooled and concentrated in a 100 K molecular weight cut-off Amicon® centrifugal filter (Millipore). The concentrated protein was loaded onto a S200 Sephacryl® XK16/100 size exclusion column (GE HealthCare Life Sciences) that had been pre-equilibrated with 50 mM MOPS, pH 7.3, 250 mM NaCl, 2 mM 2-mercaptoethanol and eluted at 0.5 mL/min with the same buffer. Protein content of the eluted fractions was assessed by SDS-PAGE. The appropriate fractions were pooled and concentrated by buffer exchange into 50 mM MOPS, pH 7.3, and stored at − 80 °C.

Oligomeric structure

Hydrodynamic radius of HFn and HFn-GE11 was determined by dynamic light scattering (DLS) using a Zetasizer Nano ZS (Malvern Instruments). The oligomeric structure of AsFe–HFn-GE11 was characterized by transmission electron microscopy (TEM). A small aliquot of a solution containing AsFe–HFn-GE11 (50 nM in 24-mer) in 50 mM MOPS, pH 7.4, was deposited onto an ultrathin holey carbon-coated copper grid (Ted Pella) and negatively stained with uranyl acetate. TEM was performed on a JEOL-2010F microscope operating at 200 kV. The image shown in Fig. 3 was obtained using a primary magnification of 150,000×.

Iron and arsenic loading of HFn and HFn-GE11

The as-isolated HFn and HFn-GE11 reproducibly contained less than 10 irons/24mer and is referred to as "empty". Iron-loaded HFn-GE11 (Fe–HFn-GE11) was prepared following a published procedure [32], which reproducibly resulted in an iron content of ~ 2500 irons per HFn 24-mer. The AsFe–HFn-GE11 was prepared using a procedure similar to that described for equine ferritin [11]. All manipulations

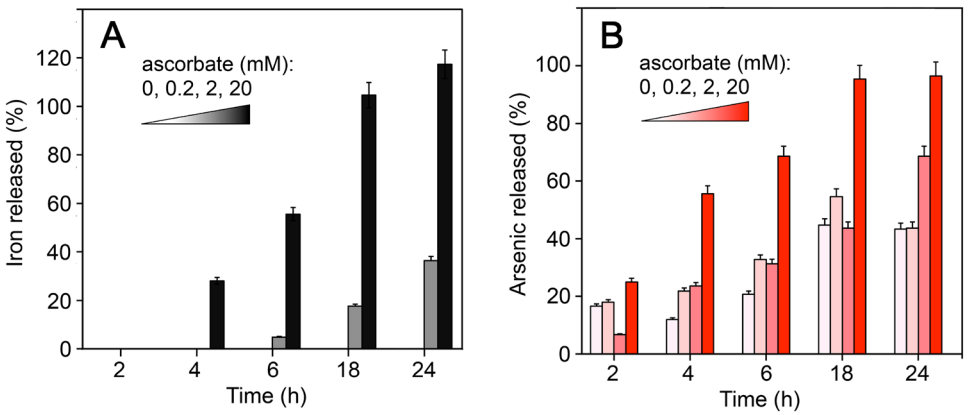

Fig. 3 Time and ascorbate concentration dependence of iron release (**a**) and arsenic release (**b**) from AsFe–Hfn-GE11. Experiments were conducted at 37 °C in anaerobic Leibovitz's L-15 medium

were performed at room temperature. A 0.02 mM ferrous ammonium sulfate solution was freshly prepared in deoxygenated ultrapure water under a N_2 atmosphere. This stock solution was used to add Fe^{2+} to an aerobic solution of 1 µM HFn-GE11 24-mer in 50 mM MOPS, 150 mM NaCl, 2 mM Na_2AsO_4, pH 7.4. Fe^{2+} was added sequentially in 200 equivalents/24-mer and incubated at room temperature for 15–20 min between additions (to allow iron to be incorporated and oxidized in the protein). Any precipitation outside the protein was removed by centrifugation (5500×*g* for 10 min). This process was repeated to achieve a total mol ratio of 2000 Fe^{2+}/HFn or HFn-GE11 24-mer in a final volume of 5 mL. Excess reagents were removed by passing the protein solution over a desalting column equilibrated with 150 mM NaCl. The iron- and arsenic-to-protein mol ratios were determined by the quantification of iron and arsenic using inductively coupled plasma-atomic emission spectroscopy (ICP-OES) and of protein using the bicinchoninic acid colorimetric assay (Pierce™ 660 nm).

Reductive iron/arsenic release

All experiments were conducted at 37 °C with no attempt to exclude air. A series of stock solutions was prepared by diluting 1:10 vol% of concentrated AsFe–HFn-GE11 in 150 mM NaCl into one of Leibovitz's L-15 medium (Gibco® L-15, ThermoFisher Scientific), 50 mM MOPS, pH 7.4, 50 mM 2-(*N*-morpholino)ethanesulfonic acid, pH 6.5, or 50 mM sodium acetate (NaAc), pH 5. After dilution all solutions contained AsFe–HFn-GE11 at 0.1 µM 24-mer. The measurements of iron and arsenic release were initiated by adding small volumes of a concentrated stock sodium ascorbate solution to 1 mL portions of HFn-GE11 stock solutions to achieve concentrations of 0, 0.2, 2, or 20 mM sodium ascorbate. The sample vials were placed in a shaking incubator at 37 °C for up to 24 h. At 2, 4, 6, 18, or 24 h after the additions of ascorbate, vials were removed from the incubator, and the protein solution was passed through a 30 kDa molecular weight cutoff centrifugal filter. The iron and arsenic in the flow-through was analyzed by ICP-OES. This procedure was repeated for separate 1 mL portions of each stock protein solution for each time point listed in the results.

Cell lines

Human mammary cancer cell lines, MDA-MB-231 (ATCC® HTB-26™) and MCF-7 (ATCC® HTB-22™), were purchased from the American Type Culture Collection. The MDA-MB-231 cells were cultured in Leibovitz's medium (Gibco® L-15, ThermoFisher Scientific) supplemented with 10% fetal bovine serum (Gibco) at 37 °C in an aerobic atmosphere incubator. MCF-7 was cultured in Minimum Essential Medium Eagle (MEME, ATTC 30-2003) without L-glutamine supplemented with 10% fetal bovine serum (Gibco), 2.0 mM Glutamax, 1.0 mM sodium pyruvate (Gibco), 0.1 mM non-essential amino acids (Gibco), 1.5 g/L sodium bicarbonate, at 37 °C in a 5% CO_2 atmosphere. Media used for confocal microscopy or cell viability assay was supplemented with penicillin–streptomycin (Pen Strep, Gibco) (100 µg/mL of penicillin, 100 µg/mL of streptomycin).

Fluorescent dye labeling of HFn and HFn-GE11

Either empty or AsFe–HFn-GE11 (0.5 µM 24-mer in 1 mL) in 50 mM MOPS, 250 mM NaCl, pH 7.4, was reacted with either Alexa Fluor™ 488 C_5 maleimide (ThermoFisher) or Cy5® maleimide (Lumiprobe GmbH) at 20 mol equiv dye/HFn monomer at room temperature for 4 h as per the manufacturer's instructions. The HFn subunit contains three Cys residues that could potentially react with the maleimide dyes. Unbound fluorophore was removed by multiple passages over Hi-Trap desalting columns. Conjugated dye per HFn 24-mer was quantified using absorbance spectroscopy and the manufacturer's published extinction coefficients to be reproducibly 20–22 dyes/24-mer.

Confocal fluorescence microscopy

The binding of either empty HFn-GE11 or AsFe–HFn-GE11 to live MDA-MB-231 cells were visualized on a Zeiss 710 confocal microscope in the University of Texas at San Antonio Biophotonics core. The C32 cells were grown in Nunc™ glass bottom Petri dishes as described above (10^6 cells per dish). The cells were treated with either Cy5-labeled empty HFn-GE11 or Cy5-labeled AsFe–HFn-GE11 to achieve a concentration of 100 nM 24-mer and incubated for various times between 0 and 12 h at 37 C under 5% CO_2. The Fe^{2+} imaging dye, Rhonox-1, was synthesized and applied to the cells according to the published methods [33], followed by treatment with immunostaining fluorescent probes (NucBlue® Live Cell Stain (Hoechst 33258) for nuclear membrane, and LysotrackDND99™ (ThermoFisher) for lysosomes, and CellMask Red™ (ThermoFisher) for plasma membrane according to the manufacturer's guidelines. After staining, the cells were washed three times with DPBS, followed by the addition of Live Cell Imaging media (ThermoFisher). All dishes were imaged on the Zeiss 710 microscope using a 63 × objective.

EC_{50}

MDA-MB-231 or MCF-7 cells were trypsinized, divided into 100,000 cells/sample, incubated for 1 h with various concentrations of Alexafluor 488-labeled HFn or HFn-GE11 and then incubated for another 20 min with propidium iodide for the quantification of cell viability. Cells were washed three times with cold phosphate-buffered saline (PBS) pelleted by centrifugation and resuspended by vortexing in Dulbecco's phosphate-buffered saline (DPBS) with 0.1% Triton X-100. For each sample, 20,000 cells were counted and analyzed using the LSR-II flow unit in the University of Texas at San Antonio Flow Cytometry Core Facility. All measurements were done in triplicate. Compensation correction, gating, and statistical data were derived using the FlowJo software. The EC_{50} values were determined by fitting a single dose–response function available in Origin (OriginLab®) to the data.

Cytotoxicities

Cell viabilities were assayed by a standard fluorescence method. Approximately 20,000 cells were seeded and cultured in the growth medium and atmosphere specified above for each cell line in black-sided, optical clear bottom, 96-well microplates. After 12 h, the medium in each plate was replaced with 100 µL fresh Pen Strep-supplemented medium containing various amounts of HFn-GE11, Fe–HFn-GE11 or AsFe–HFn-GE11 to achieve final concentrations between 0 and 100 nM 24-mer. The plates were placed in 37 °C incubators under either aerobic (MDA-MB-231) or 5% CO_2 atmospheres (MCF-7) for 48 h. The medium was then decanted, and cells were washed twice with Hank's balanced salt solution. Cell viability was measured using the CyQuant NF® assay (Life Technologies™). The fluorescent substrate was added as per the manufacturer's instructions, the plate was incubated for 30 min at 37 °C, and the fluorescence emission measured at 520 nm (excitation at 480 nm) on a SpectraMax® plate reader. All experiments were performed in multiples of eight. Parallel control experiments were conducted by treating the cells with ATO, sodium arsenate, or ferrous ammonium sulfate in place of the AsFe–HFn-GE11. IC_{50} values were determined by fitting of a single dose–response function to the data in Origin®. Significant differences in the fitted IC_{50} values were assessed using the ANOVA test ($p < 0.05$).

Results

As shown schematically in Fig. 2, we extended the C-terminal end of the HFn subunit with GE11 (HFn-GE11). The magenta-colored portion at the center of Fig. 1a shows one of the six locations where we expect four GE11 peptides to protrude from the outer surface of HFn-GE11 [22, 23, 34]. We expressed and isolated HFn and HFn-GE11 using *E. coli* expression plasmids and standard purification protocols, then loaded the HFn and HFn-GE11 with arsenate and iron to the published levels [11]. We refer to the arsenate/$[FeO(OH)]_n$-loaded protein as AsFe–HFn-GE11. For comparison, we used the non-loaded HFn-GE11("empty") and iron-only-loaded protein (Fe–HFn-GE11).

DLS (Fig. S1A) showed that the HFn-GE11 formed a stable monodisperse 24-mer with a slightly larger diameter (16 nm) than that of HFn (13 nm), as expected if the 24 linker-GE11 peptides were protruding from the outer surface of the protein shell. Transmission electron microscopy (Fig. S1B) showed that the HFn-GE11 retained the characteristic spherical shape of ferritin. We were able to load HFn-GE11 with arsenate and iron to the published levels [11] (700–800 arsenic and 1600–1700 iron per 24-mer, quantified by ICP-OES).

Under anaerobic conditions, ascorbate induced little or no iron release from horse spleen ferritin [35, 36]. This observation led us to test the possibility that ascorbate could differentiate the time courses of reductive iron and arsenic release from AsFe–Hfn-GE11. For these tests, we used anaerobic Leibovitz's L-15 medium, which contains biological factors, such as ~ 2 mM phosphate, which could conceivably displace arsenate, and ~ 1 mM L-cysteine, a potential reducing agent. Figure 3a, b shows that at either 0 or 0.2 mM ascorbate, the latter of which is the normal maximum blood concentration [37], less than 50% of the arsenic and little or no iron was

released after 24 h, a time interval within which, according to published work, HFn can localize to mouse xenograft tumors after intravenous injection [14]. Release of iron as Fe^{2+} from AsFe–HFn-GE11 became evident only at or above 2 mM ascorbate; full release of both iron and arsenic required 20 mM ascorbate and at least 18 h. We found that in the presence of 20 mM ascorbate both arsenic and iron were released more rapidly at lower pHs (Fig. S2). As described below, this pH dependence may be an advantage for intracellular iron and arsenic release.

Flow cytometry results (Fig. 4) showed that HFn-GE11 (EC_{50} = 47 nM) had an approximately sixfold higher affinity than HFn (EC_{50} = 280 nM) for the EGFR-hyperexpressing triple-negative breast cancer cell line, MDA-MB-231. Live cell confocal fluorescence microscopy (LCCFM) (Fig. 5) showed that both HFn-GE11 and AsFe–HFn-GE11 were endocytosed by MDA-MB-231 and localized to the lysosomes within 1 h after addition of either protein. Release of iron was observable using an Fe^{2+}-specific imaging dye [33] within 1 h of exposure of cells to the arsenic, iron-loaded protein, whereas no intracellular Fe^{2+} was observable over the same time period upon treatment with the empty protein.

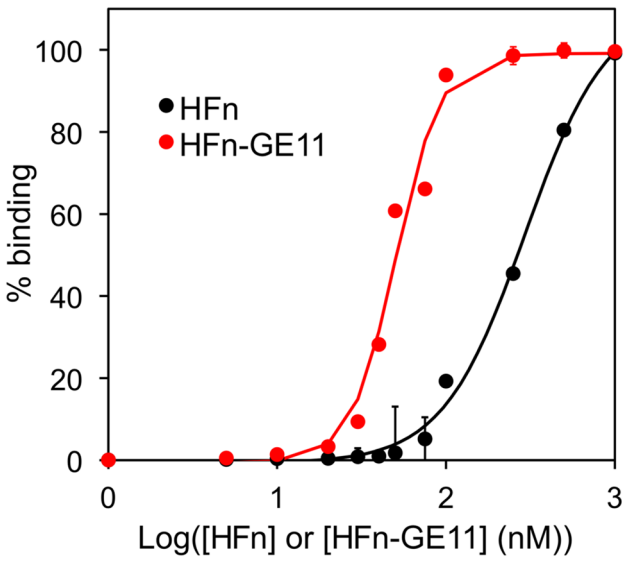

Fig. 4 Flow cytometry for binding of HFn and HFn-GE11 to MDA-MBA-231 cells. Data points are the average of at least three determinations with error bars representing standard deviations

LCCFM images at either 2 or 12 h after treatment with AsFe–HFn-GE11 (Fig. 6) show increasing amounts of Fe^{2+} in the cytoplasm. This observation indicates that the iron in the AsFe–HFn-GE11 core can be reduced after AsFe–HFn-GE11 enters the lysosomes and can then diffuse out. Based on the relative iron and arsenic release rates from AsFe–HFn-GE11 in Fig. 3a vs Fig. 3b, we expect even faster intracellular release of arsenic.

MDA-MD-23 cell viabilities are shown in Fig. 7 and corresponding IC_{50} values are listed in Table 1. The IC_{50} of 10 nM 24-mer for AsFe–HFn-GE11 corresponds to an added arsenic concentration of 8 µM, which is similar to the IC_{50} we obtained for ATO (~ 5 µM As, Fig. 7b; Table 1) under the same conditions and also to values reported in the literature for ATO on the same cell line (2–7 µM As) [5, 38]. Under similar conditions MDA-MB-231 showed little or no sensitivity to the empty HFn-GE11 or to Fe–HFn-GE11 up to 1000 nM 24-mer. The arsenic cargo is thus required for effective cytotoxicity. Moreover, we observed a > eightfold *lower* cytotoxicity for added 'free' inorganic arsenate compared to AsFe–Hfn on an [As] basis (Fig. 7; Table 1). These results indicate a more efficient uptake and/or intracellular reduction of the arsenate prodrug when delivered by the HFn-GE11 cage.

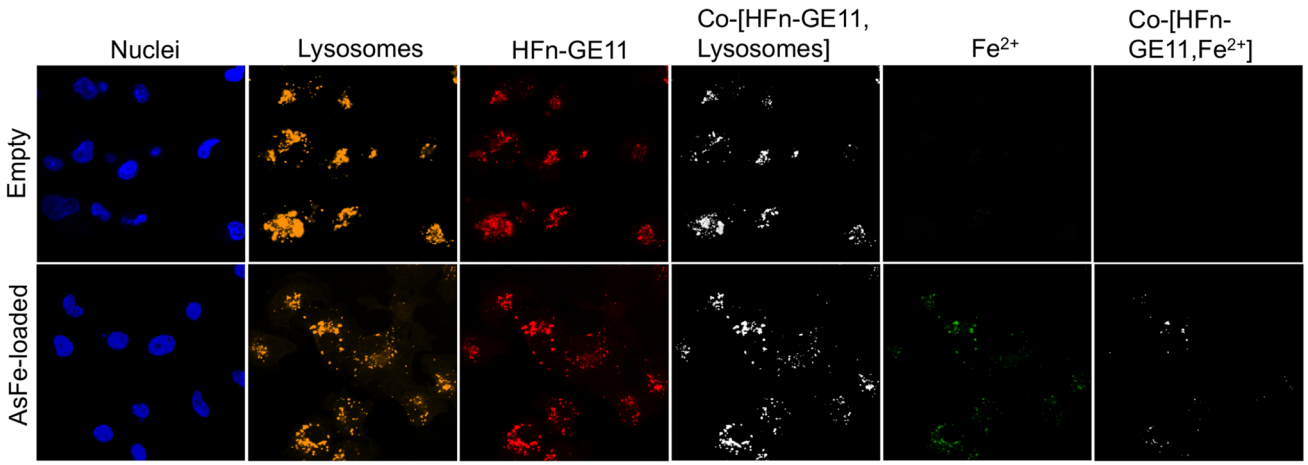

Fig. 5 LCCFM of MDA-MB-231 cells ~ 1 h after addition of Cy5-labeled empty or AsFe–HFn-GE11 to a concentration of approximately ~ 1 µM. Column headings indicate organelle, Cy5-labeled Hfn-GE11, or Fe^{2+} fluorescence detection. 'Co-' prefix indicates overlay of the indicated pairs of images, demonstrating co-localization

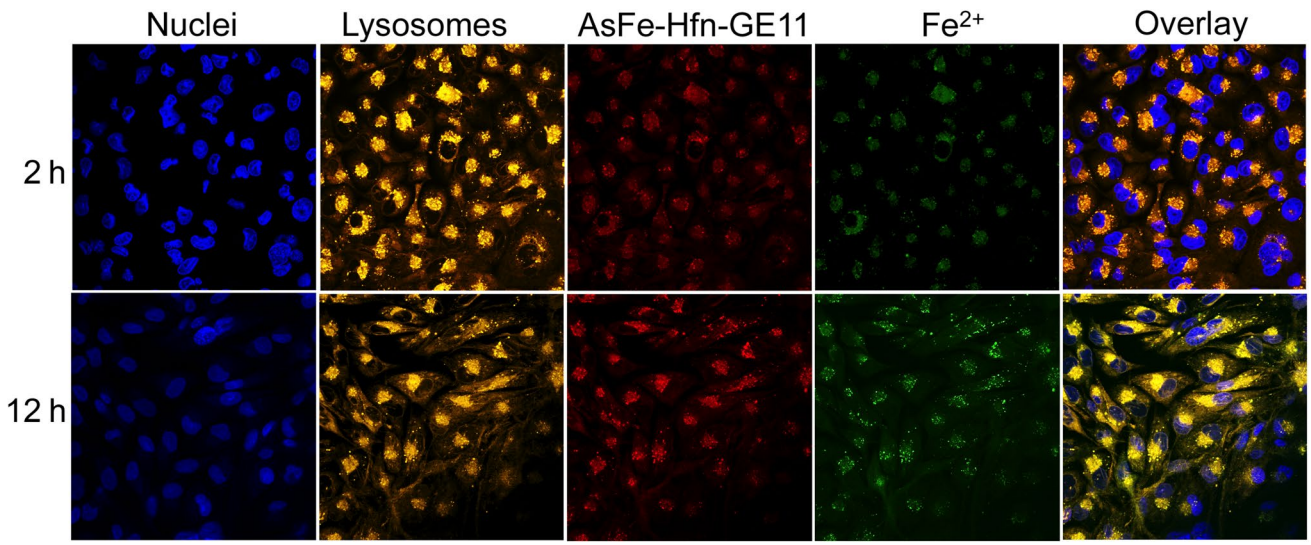

Fig. 6 LCCFM of MDA-MB-231 either 2 or 12 h after addition of AsFe–HFn-GE11 to a concentration of ~ 1 µM

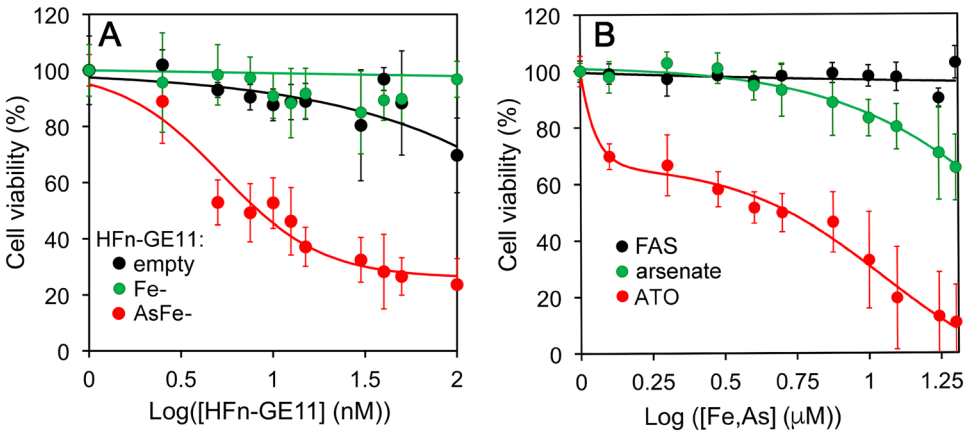

Fig. 7 MDA-MB-231 cell viabilities 48 h after addition of various concentrations of **a** empty, Fe–Hfn-GE11, or AsFe–HFn-GE11 or **b** ferrous ammonium sulfate (FAS), ATO, or sodium arsenate. Data points are the average of eight determinations with error bars representing standard deviations

Table 1 IC_{50} values for empty Hfn-GE11, Fe–Hfn-GE11, AsFe–Hfn-GE11, ATO or arsenate

Cell line	Treatment				
	HFn-GE11 species			ATO	Arsenate
	Empty	Fe-	AsFe-		
MDA-MB-231	> 1[a]	> 1[a]	8	5	> 60
MCF-7	> 1[a]	> 1[a]	85	43	1800

IC_{50} values for arsenic-containing species are listed on the basis of micromolar total arsenic concentration

[a]In micromolar Hfn-GE11 24-mer species

For the relatively low EGFR-expressing breast cancer cell line, MCF-7, we found that HFn-GE11 bound with an EC_{50} = 92 nM 24-mer, which was threefold *lower* than IC_{50} for the parent HFn (IC_{50} = 28 nM) (Fig. S3A). The GE11 peptide thus appeared to *decrease* the affinity of Hfn for MCF-7, possibly by hindering interaction with the Trf1 receptor. MCF-7 showed an order of magnitude lower sensitivity to AsFe–HFn-GE11 (IC_{50} = 106 nM 24-mer, ~ 85 µM As; Fig. S3B) than did MDA-MB-231. Under our culture conditions, MCF-7 also showed a lower sensitivity to ATO (IC_{50} = 43 µM As; Fig. S3C) compared to that of MDA-MB-231. Table 1 summarizes the cytotoxicity results for the two cell lines.

Discussion

Our results demonstrate proof-of-concept for a novel approach to targeted cancer cell killing according to the mechanism illustrated in Fig. 2a. The presence of the GE11 peptide on Hfn led to the expected higher affinity for the high EGFR-expressing MDA-MB-231 cell line (Fig. 4) than for the relatively low EGFR-expressing MCF-7 cell

line (Fig. S3). As expected, the HFn-GE11 localized preferentially into lysosomes, from which we observed released Fe^{2+} radiating outward through the cell (Figs. 5, 6). The arsenate/ferric oxyhydroxide "prodrug" cargo within the HFn-GE11 protein shell is thus endocytosed prior to its reductive release of Fe^{2+}. Based on the relative reductive iron vs arsenic release rates from HFn-GE11 (Figs. 3, S2), we infer faster intracellular release and distribution of ATO. This reductive arsenic release scenario is further supported by the striking similarities of the arsenic IC_{50} values for AsFe–Hfn-GE11 and free ATO on both breast cancer cell lines, and the much higher IC_{50} values for 'free' inorganic arsenate (Figs. 7, S3; Table 1). (Unfortunately, there appear to be no reliable methods for LCCFM imaging of intracellular arsenate or ATO.) These observations together with the rapid uptake of Hfn-GE11 by the cells (Fig. 5) are *not consistent* with a cytotoxicity mechanism in which (1) arsenate is released from AsFe–Hfn-GE11 outside the cell, (2) the released extracellular arsenate is reduced to ATO, and (3) the ATO is then taken up by the cells. Arsenate loading into Hfn-GE11 was required for effective cell killing. The iron-only-loaded Hfn-GE11 was not detectably cytotoxic up to 1 μM 24-mer (Fig. 7a; Table 1). This "Trojan horse" approach to intracellular delivery of arsenate and reductive release as ATO could conceivably be adapted for the treatment of other cancers with targetable cell or vascular receptors [8, 39]. Hfn has proven to be a versatile scaffold for the delivery of various drugs and imaging cargo to cells [17]. We can thus, envision expansion of our reductive delivery of ATO to anticancer combination therapies using Hfn [3, 40].

Acknowledgements This article is dedicated to the memory of Beth A. Goins. This research was supported by a Grant from the Cancer Prevention and Research Institute of Texas (RP110165). The Biophotonics Core facility and Flow Cytometry Core facility at the University of Texas at San Antonio (UTSA) are supported by a Grant from the National Institute on Minority Health and Health Disparities from the National Institutes of Health (G12MD007591). H. Shipley in the UTSA Department of Civil and Environmental Engineering, and K. Nash in the UTSA Department of Physics and Astronomy provided access to ICP-OES and DLS instrumentation, respectively.

Compliance with ethical standards

Conflict of interest The authors declare no conflicts of interest.

References

1. Liu JX, Zhou GB, Chen SJ, Chen Z (2012) Curr Opin Chem Biol 16:92–98
2. Swindell EP, Hankins PL, Chen H, Miodragovic DU, O'Halloran TV (2013) Inorg Chem 52:12292–12304
3. Hoonjan M, Jadhav V, Bhatt P (2018) J Biol Inorg Chem 23:313–329
4. Zangi R, Filella M (2012) Chem-Biol Interact 197:47–57
5. Ahn RW, Chen F, Chen H, Stern ST, Clogston JD, Patri AK, Raja MR, Swindell EP, Parimi V, Cryns VL, O'Halloran TV (2010) Clin Cancer Res 16:3607–3617
6. Zhao ZH, Zhang H, Chi XQ, Li H, Yin ZY, Huang DT, Wang XM, Gao JH (2014) J Mater Chem B 2:6313–6323
7. Zhao Z, Wang X, Zhang Z, Zhang H, Liu H, Zhu X, Li H, Chi X, Yin Z, Gao J (2015) ACS Nano 9:2749–2759
8. Wu X, Han Z, Schur RM, Lu Z-R (2016) ACS Biomater Sci Eng 2:501–507
9. Akhtar A, Wang SX, Ghali L, Bell C, Wen X (2017) J Biomed Res 31:177–188
10. Ebrahimi KH, Hagedoorn PL, Hagen WR (2015) Chem Rev 115:295–326
11. Polanams J, Ray AD, Watt RK (2005) Inorg Chem 44:3203–3209
12. Nemeti B, Gregus Z (2002) Toxicol Sci 70:4–12
13. Watt GD, Frankel RB, Papaefthymiou GC, Spartalian K, Stiefel EI (1986) Biochemistry 25:4330–4336
14. Liang M, Fan K, Zhou M, Duan D, Zheng J, Yang D, Feng J, Yan X (2014) Proc Natl Acad Sci USA 111:14900–14905
15. Hasan MR, Tosha T, Theil EC (2008) J Biol Chem 283:31394–31400
16. Masuda T, Goto F, Yoshihara T, Mikami B (2010) Biochem Biophys Res Commun 400:94–99
17. Truffi M, Fiandra L, Sorrentino L, Monieri M, Corsi F, Mazzucchelli S (2016) Pharmacol Res 107:57–65
18. Li L, Fang CJ, Ryan JC, Niemi EC, Lebron JA, Bjorkman PJ, Arase H, Torti FM, Torti SV, Nakamura MC, Seaman WE (2010) Proc Natl Acad Sci USA 107:3505–3510
19. Vannucci L, Falvo E, Fornara M, Di Micco P, Benada O, Krizan J, Svoboda J, Hulikova-Capkova K, Morea V, Boffi A, Ceci P (2012) Int J Nanomed 7:1489–1509
20. Zhen ZP, Tang W, Chen HM, Lin X, Todd T, Wang G, Cowger T, Chen XY, Xie J (2013) ACS Nano 7:4830–4837
21. Uchida M, Flenniken ML, Allen M, Willits DA, Crowley BE, Brumfield S, Willis AF, Jackiw L, Jutila M, Young MJ, Douglas T (2006) J Am Chem Soc 128:16626–16633
22. Lee JH, Seo HS, Song JA, Kwon KC, Lee EJ, Kim HJ, Lee EB, Cha YJ, Lee J (2013) ACS Nano 7:10879–10886
23. Lee EJ, Lee SJ, Kang YS, Ryu JH, Kwon KC, Jo E, Yhee JY, Kwon IC, Kim K, Lee J (2015) Adv Funct Mat 25:1279–1286
24. Roskoski R Jr (2014) Pharmacol Res 79:34–74
25. Park HS, Jang MH, Kim EJ, Kim HJ, Lee HJ, Kim YJ, Kim JH, Kang E, Kim SW, Kim IA, Park SY (2014) Modern Pathol 27:1212–1222
26. Nakajima H, Ishikawa Y, Furuya M, Sano T, Ohno Y, Horiguchi J, Oyama T (2014) Breast Cancer 21:66–74
27. Kalimutho M, Parsons K, Mittal D, Lopez JA, Srihari S, Khanna KK (2015) Trends Pharmacol Sci 36:822–846
28. Mickler FM, Mockl L, Ruthardt N, Ogris M, Wagner E, Brauchle C (2012) Nano Lett 12:3417–3423
29. Tang H, Chen X, Rui M, Sun W, Chen J, Peng J, Xu Y (2014) Mol Pharmaceut 11:3242–3250
30. Song S, Liu D, Peng J, Sun Y, Li Z, Gu JR, Xu Y (2008) Int J Pharmaceut 363:155–161
31. Tabor S (1990) In: Ausubel FA, Brent R, Kingston RE, Moore DD, Seidman JG, Smith JA, Struhl K (eds) Current protocols in molecular biology. Wiley, New York, pp 16.12.11–16.12.11
32. Baaghil S, Lewin A, Moore GR, Le Brun NE (2003) Biochemistry 42:14047–14056
33. Hirayama T, Okuda K, Nagasawa H (2013) Chem Sci 4:1250–1256
34. Lee BR, Ko HK, Ryu JH, Ahn KY, Lee YH, Oh SJ, Na JH, Kim TW, Byun Y, Kwon IC, Kim K, Lee J (2016) Sci Rep 6:35182
35. Ahmad S, Kitchin KT, Cullen WR (2000) Arch Biochem Biophys 382:195–202

36. Bienfait HF, van den Briel ML (1980) Biochim Biophys Acta 631:507–510
37. Ma Y, Chapman J, Levine M, Polireddy K, Drisko J, Chen Q (2014) Sci Transl Med 6:222ra218
38. Baj G, Arnulfo A, Deaglio S, Mallone R, Vigone A, De Cesaris MG, Surico N, Malavasi F, Ferrero E (2002) Breast Cancer Res Treat 73:61–73
39. Zhang L, Zhang Z, Mason RP, Sarkaria JN, Zhao D (2015) Sci Rep 5:9874
40. Miodragovic D, Swindell EP, Waxali ZS, Bogachkov A, O'Halloran TV (2019) Inorg Chim Acta 496:119030

Affiliations

Daniela Cioloboc[1] · Donald M. Kurtz Jr.[1]

✉ Donald M. Kurtz Jr.
donald.kurtz@utsa.edu

[1] Department of Chemistry, University of Texas at San Antonio, San Antonio, TX, USA